2930 *Chem. Mater.* **2009,** *21,* 2930–2934
DOI:10.1021/cm9007409

CHEMISTRY OF MATERIALS
Article

Highly Polarized and Self-Waveguided Emission from Single-Crystalline Organic Nanobelts

Yanke Che,[†] Xiaomei Yang,[†] Kaushik Balakrishnan,[‡] Jianmin Zuo,[§] and Ling Zang*[,†]

[†]*Department of Materials Science and Engineering, University of Utah, 383 Colorow Drive, Salt Lake City, Utah 84108,* [‡]*Department of Chemistry, Rice University, Houston, Texas 77005, and* [§]*Department of Materials Science and Engineering, University of Illinois at Urbana−Champaign, Urbana, Illinois 61801*

Received March 17, 2009. Revised Manuscript Received April 29, 2009

Well-defined single-crystalline nanobelts with strong fluorescence were fabricated from a perylene tetracarboxylic diimide molecule modified with specific side-chains that afford flip-flap stacking, rather than the common translated stacking, between the molecules along the long axis of the nanobelt. The nanobelts thus fabricated possess highly polarized, self-waveguided emission, making them ideal candidates for application in nanolasers and other angle-dependent optical nanodevices.

Introduction

Inorganic nanowires have been extensively investigated for the linear optical properties, which can potentially be employed in various nanodevice applications including laser, waveguide, and polarized emission.[1−5] In contrast, the same research has been much less advanced for the organic counterparts, mainly because of the technical challenges in control and optimization of one-dimensional (1D) self-assembly of organic molecules.[6] Moreover, the device application concerned with the linear optical properties (particularly those based on fluorescence emission) demands that the organic nanomaterials thus fabricated be highly fluorescent.[7−9] Although various oligomers,[10] conjugated polymers,[11−13] and low-weight small molecules[6,10] have been fabricated into 1D nanostructures, most of the π-conjugated molecules lose their strong fluorescence upon being assembled into the solid state.[14−16] This is particularly true for the planar, disklike molecules, which are usually suited for 1D self-assembly through the $\pi-\pi$ stacking.[6,17] The challenge is thus to find building-block molecules that are not only suited for fabrication into 1D structure but also, even more importantly, enable strong fluorescence in the solid state. Among the organic nanomaterials previously fabricated, few demonstrated efficient fluorescent emission.[7−9,18−22]

Perylene-carboxylic diimides (PTCDI) represent a robust class of n-type organic semiconductor with high thermal and photostability, and have long been used in various optoelectronic devices.[6,17,23] As recently evidenced, appropriate side-chain modification of PTCDI molecules enables 1D self-assembly into well-defined nanowires or nanobelts.[24−26] However, none of these 1D nanomaterials demonstrate sufficient fluorescence emission that can potentially be employed in real devices. Although highly fluorescent organogels can feasibly be fabricated from the PTCDIs modified with substituents at the bay positions,[27] the twisted-conformation of the PTCDI backbone distorts the $\pi-\pi$ stacking, thus preventing the formation of well-defined

*Corresponding author. E-mail: lzang@eng.utah.edu.

(1) Xia, Y.; Yang, P.; Sun, Y.; Wu, Y.; Mayers, B.; Gates, B.; Yin, Y.; Kim, F.; Yan, H. *Adv. Mater.* **2003**, *15*, 353–389.
(2) Huang, M. H.; Mao, S.; Feick, H.; Yan, H.; Wu, Y.; Kind, H.; Weber, E.; Russo, R.; Yang, P. *Science* **2001**, *292*, 1897–9.
(3) Law, M.; Sirbuly, D. J.; Johnson, J. C.; Goldberger, J.; Saykally, R. J.; Yang, P. *Science* **2004**, *305*, 1269–1273.
(4) Agarwal, R.; Barrelet, C. J.; Lieber, C. M. *Nano Lett.* **2005**, *5*, 917–920.
(5) Wang, J.; Gudiksen, M. S.; Duan, X.; Cui, Y.; Lieber, C. M. *Science* **2001**, *293*, 1455–7.
(6) Zang, L.; Che, Y.; Moore, J. S. *Acc. Chem. Res.* **2008**, *41*, 1596–1608.
(7) Zhao, Y. S.; Fu, H.; Hu, F.; Peng, A.; Yang, W.; Yao, J. *Adv. Mater.* **2008**, *20*, 79–83.
(8) Quochi, F.; Cordella, F.; Mura, A.; Bongiovanni, G.; Balzer, F.; Rubahn, H. G. *Appl. Phys. Lett.* **2006**, *88*, 041106/1–041106/3.
(9) Zhao, Y. S.; Peng, A.; Fu, H.; Ma, Y.; Yao, J. *Adv. Mater.* **2008**, *20*, 1661–1665.
(10) Hoeben, F. J. M.; Jonkheijm, P.; Meijer, E. W.; Schenning, A. P. H. J. *Chem. Rev.* **2005**, *105*, 1491–1546.
(11) O'Carroll, D.; Lieberwirth, I.; Redmond, G. *Nat. Nanotechnol.* **2007**, *2*, 180–184.
(12) Li, D.; Huang, J.; Kaner, R. B. *Acc. Chem. Res.* **2009**, *42*, 135–145.
(13) Lee, M.; Cho, B.-K.; Zin, W.-C. *Chem. Rev.* **2001**, *101*, 3869–3892.
(14) Jenekhe, S. A.; Osaheni, J. A. *Science* **1994**, *265*, 765–8.
(15) Langhals, H.; Krotz, O.; Polborn, K.; Mayer, P. *Angew. Chem., Int. Ed.* **2005**, *44*, 2427–2428.
(16) Cornil, J.; Beljonne, D.; Calbert, J.-P.; Bredas, J.-L. *Adv. Mater.* **2001**, *13*, 1053–1067.
(17) Wurthner, F. *Chem. Commun.* **2004**, 1564–79.
(18) Xie, Z.; Yang, B.; Li, F.; Cheng, G.; Liu, L.; Yang, G.; Xu, H.; Ye, L.; Hanif, M.; Liu, S.; Ma, D.; Ma, Y. *J. Am. Chem. Soc.* **2005**, *127*, 14152–14153.
(19) Coropceanu, V.; Cornil, J.; Da Silva Filho, D. A.; Olivier, Y.; Silbey, R.; Bredas, J.-L. *Chem. Rev.* **2007**, *107*, 926–952.
(20) An, B. K.; Lee, D. S.; Lee, J. S.; Park, Y. S.; Song, H. S.; Park, S. Y. *J. Am. Chem. Soc.* **2004**, *126*, 10232–10233.
(21) Naddo, T.; Che, Y.; Zhang, W.; Balakrishnan, K.; Yang, X.; Yen, M.; Zhao, J.; Moore, J. S.; Zang, L. *J. Am. Chem. Soc.* **2007**, *129*, 6978–6979.
(22) Ajayaghosh, A.; Praveen, V. K. *Acc. Chem. Res.* **2007**, *40*, 644–656.
(23) Newman, C. R.; Frisbie, C. D.; da Silva Filho, D. A.; Bredas, J.-L.; Ewbank, P. C.; Mann, K. R. *Chem. Mater.* **2004**, *16*, 4436–4451.
(24) Che, Y.; Datar, A.; Balakrishnan, K.; Zang, L. *J. Am. Chem. Soc.* **2007**, *129*, 7234–7235.
(25) Balakrishnan, K.; Datar, A.; Naddo, T.; Huang, J.; Oitker, R.; Yen, M.; Zhao, J.; Zang, L. *J. Am. Chem. Soc.* **2006**, *128*, 7390–7398.
(26) Balakrishnan, K.; Datar, A.; Oitker, R.; Chen, H.; Zuo, J.; Zang, L. *J. Am. Chem. Soc.* **2005**, *127*, 10496–10497.
(27) Li, X.-Q.; Zhang, X.; Ghosh, S.; Wuerthner, F. *Chem.–Eur. J.* **2008**, *14*, 8074–8078.

Published on Web 05/11/2009

nanowires in straight geometry suited for nanodevices fabrication.

It is well-proven that the side-chains of PTCDIs play a vital role in controlling the molecular packing, and thus the morphology, as well as the optoelectronic properties of the assembled materials.[6,25,28,29] Appropriate side-chain modification enables a good balance between maintaining effective molecular stacking and the desired strong fluorescence of the materials thus assembled. The former usually dictates the 1D growth of the molecular assembly (which in turn prefers a molecular structure with minimal steric hindrance), whereas the latter usually favors bulky, steric side-chains that may distort the $\pi-\pi$ stacking to afford increased fluorescence (by enhancing the low-energy excitonic transition) for the molecular assembly.[6,17,25,28,30,31] These two requirements result in a situation where one property is maximized at the expense of the other for the same molecule. Strong fluorescent nanofibers have recently been fabricated from a half-hydrolyzed PTCDI modified with branched side-chains in appropriate size (e.g., hexylheptyl).[28] However, the nanofibers fabricated are highly curved and entangled together, likely because of the asymmetric structure of the molecules. Although the entangled nanofibers demonstrate potential applications in fluorescence sensing of gaseous reagents,[28] the curved shape makes them less-suited for application in 1D confined optical nanodevices. Herein, we report on fabrication of shape-defined nanobelts from the flip-flap stacking of a cyclohexyl substituted molecule, CH-PTCDI, as shown in Chart 1. The nanobelts fabricated are of pure single-crystalline phase and demonstrate strong, polarized fluorescence. More interestingly, the fluorescence can be self-guided in high efficiency along the long axis of the nanobelt. Combination of these features makes the nanobelts ideal for application in a variety of optoelectronic nanodevices, such as polarized OLEDs,[32] waveguides[8,33,34] and laser materials,[8,9,11] where 1D confined optical properties are highly demanded.

Results and Discussion

As shown in Figure 1, well-defined nanobelts have been fabricated from the symmetric CH-PTCDI as evidenced by both SEM and TEM imaging. The fabrication was performed through a so-called phase-transfer process,[6] in which the self-assembly of the molecules occurs at the interface between a "poor" and "good" solvent (see the Supporting Information). The nanobelts demonstrate long, straight belt-like morphology with length of hundreds of micrometers and width of 250 to 1500 nm (also shown in Figures S1 and S2 of the Supporting Information). The thickness of the nanobelts is ca. 100 nm,[35] which can be clearly seen from the cross-section of broken nanobelts (see Figure S2 in the Supporting Information). The beltlike morphology is also evidenced by the TEM imaging over a single nanobelt deposited on holey carbon film (Figure 1B), where even contrast was observed across the whole belt surface. Electron diffraction of this nanobelt showed a typical single-crystalline pattern with sharp diffraction spots, in which two distinct, orthogonal reciprocal lattice vectors can be obtained from the diffraction pattern, giving two d-spacings, d_1 = 7.15 Å

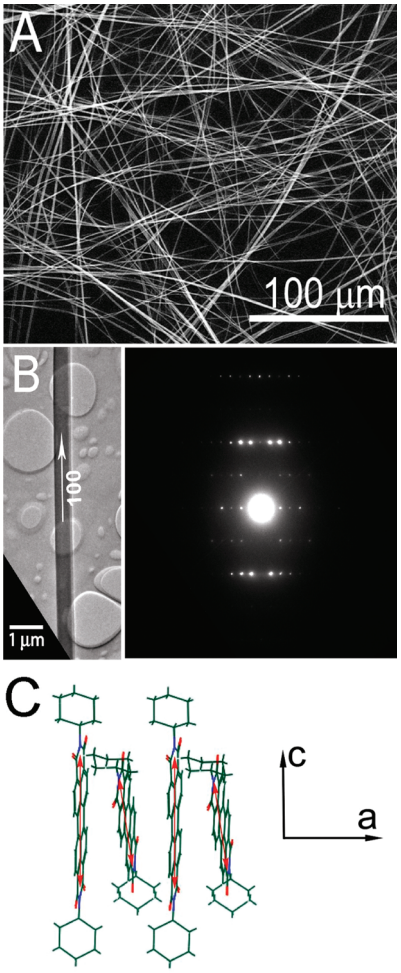

Figure 1. (A) Large area SEM image showing the long nanobelts deposited on a glass slide; (B) (left) TEM image of a nanobelt cast on carbon film, (right) electron diffraction recorded over the nanobelt; (C) a schematic diagram showing the flip-flap molecular stacking along the *a*-axis, i.e., the long axis of the nanobelt. The red arrow indicates the direction of the transition dipole moment of the molecule.

Chart 1

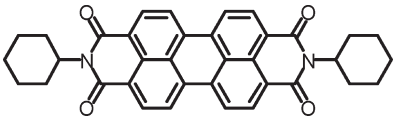

(28) Che, Y.; Yang, X.; Loser, S.; Zang, L. *Nano Lett*. **2008**, *8*, 2219–2223.
(29) Kazmaier, P. M.; Hoffmann, R. *J. Am. Chem. Soc*. **1994**, *116*, 9684–91.
(30) Thomas, S. W.; Joly, G. D.; Swager, T. M. *Chem. Rev*. **2007**, *107*, 1339–1386.
(31) Ahrens, M. J.; Sinks, L. E.; Rybtchinski, B.; Liu, W.; Jones, B. A.; Giaimo, J. M.; Gusev, A. V.; Goshe, A. J.; Tiede, D. M.; Wasielewski, M. R. *J. Am. Chem. Soc*. **2004**, *126*, 8284–8294.
(32) Sakamoto, K.; Miki, K.; Misaki, M.; Sakaguchi, K.; Chikamatsu, M.; Azumi, R. *Appl. Phys. Lett*. **2007**, *91*, 183509/1–183509/3.
(33) Takazawa, K.; Kitahama, Y.; Kimura, Y.; Kido, G. *Nano Lett*. **2005**, *5*, 1293–1296.
(34) Balzer, F.; Bordo, V. G.; Simonsen, A. C.; Rubahn, H. G. *Appl. Phys. Lett*. **2003**, *82*, 10.

(35) It is generally accepted in the field of nanotechnology that materials with at least one dimension in the size range of 1−100 nm can be referred to as nanoscale materials.

and d_2 = 21.41 Å, corresponding to the *a* and *c* crystal axes, respectively.

CH-PTCDI molecules are expected to take a flip-flap stacking (as shown in Figure 1C) to minimize the steric hindrance between the cyclohexyl side-chains, which are crossed to the molecular plane at about 90°. The translated stacking (with both longitudinal and transverse sliding), which has been commonly observed for many other PTCDI molecules,[29,36] is apparently implausible for CH-PTCDI, mainly because of the unfavorable intermolecular contact caused by the bulky side-chains when compressed within the typical $\pi-\pi$ stacking distance (~3.5 Å). The flip-flap intermolecular stacking is also consistent with the energy minimization calculations performed on a stacked dimer at a fixed stacking distance, 3.5 Å, for which the total energy of the dimer decreases sharply upon rotating the molecule from the eclipsed stacking, and reaches the most stable stacking conformation at rotated angle of 40° (see Figure S3 in the Supporting Information). Although the exactly crossed stacking (rotated at 90 degree) is also referred to as an energy minimal point, it is unlikely adopted in the crystalline packing mainly considering the higher symmetry of the stacking (D_{4h}, viewed from the stacking direction), which should, however, lead to formation of nanorods with approximately round shape cross-section, rather than the beltlike morphology as indeed observed herein. Interestingly, the calculated transition dipole moment of the flip-flap stacking (see Figure S4 in the Supporting Information) is completely confined in the molecular plane with distribution along both the long (*X*) and short (*Y*) axis. Such an in-plane confinement makes the transition dipole moment of the nanobelt approximately perpendicular to the stacking direction, i.e., the long axis of the nanobelt, as indeed observed in the polarized emission measurement (vide infra). This observation is in sharp contrast to the molecular arrangement adopting translated stacking, for which the transition dipole moment can be tilted out of the molecular plane, turning parallel to the stacking direction, as indeed observed for some of the PTCDI nanowires.[6] The *d*-spacing of 7.15 Å measured from the electron diffraction (Figure 1B) is also supportive for the flip-flap stacking, for which the shortest distance between two identical molecules in the crystal unit is actually double the intermolecular $\pi-\pi$ stacking distance (as depicted in Figure 1C), which is typically around 3.5 Å. Such double-stacking *d*-spacing was also observed for other PTCDI molecules modified with cross-linked bulky side-chains, which adopted the similar flip-flap crystalline stacking.[36,37] However, no one-dimensional self-assembly has ever been achieved for these molecules.

The measured *d*-spacings are also consistent with the X-ray diffraction (XRD) measurement of the nanobelts (Figure S5), which was carried out using the synchrotron X-ray beam from the APS, Argonne National Lab. The well-defined, sharp peaks shown in the XRD spectrum are indicative of the single crystalline structure of the nanobelts, for which the $\pi-\pi$ stacking (with the characteristic *d*-spacing of 3.49 Å) was clearly revealed. The other two *d*-spacings deduced from the XRD spectrum, 7.0 Å (100) and 10.6 Å (002), are consistent with the results obtained from the E-diffraction as described above, for which (100) refers to the a crystal axis and (001) refers to the *c* axes. The $\pi-\pi$ stacking is also supported by the UV/vis and luminescence spectra, where the strong $\pi-\pi$ stacking leads to significant red-shift in both the absorption (27 nm) and fluorescence spectrum (99 nm) compared to the free CH-PTCDI molecules dissolved in solutions (seee Figure S6 in the Supporting Information). The single-crystalline phase of the nanobelts was also evidenced from the multipoint electron diffraction measurement performed at different positions along the long axis of the nanobelt using the electron nanobeam technique,[38,39] for which the identical electron diffraction patterns were obtained throughout the whole nanobelt (see Figure S7 in the Supporting Information).

In contrast to the weak fluorescence emission (with quantum yield $<1\%$) previously observed for the self-assembled materials of PTCDIs, which mostly adopted the translated stacking,[26] the nanobelts reported herein demonstrate dramatically increased emission (with quantum yield of ca. 17%), which can easily be imaged with a fluorescence microscope (Figure 2A). The increased fluorescence of these new nanobelts is apparently due to the flip-flap stacking mode, which was believed to be effective for enhancing the fluorescence by strengthening the low-energy excitonic transition.[16,40] Similar enhancement in fluorescence was also observed in other types of molecules that adopted flip-flap stacking.[18] The strong emission, along with the single crystalline phase (dominated by the $\pi-\pi$ stacking) and the large Stokes shift, makes the nanobelts ideal materials module for polarized, self-waveguided emission.[33] Indeed, highly polarized emission was observed for the nanobelts as depicted in the inset of Figure 2A. Careful study showed that the most intense emission was obtained when the polarizer was placed at approximately 82° with respect to the long axis of the nanobelts, while the emission intensity diminished to the minimal upon rotating the polarizer by 90° from this position (Figure 2B). The emission polarization thus observed, approximately perpendicular to the long axis of the nanobelt, is consistent to the theoretical calculation based on the molecular stack (see Figure S4 in the Supporting Information), for which the transition dipole moment is completely confined within the molecular plane. The maximal/minimal intensity ratio (I_{max}/I_{min}) as detected in Figure 2B was about 10, producing a polarization factor, $(I_{max} - I_{min})/(I_{max} + I_{min})$, of ca. 82%. Such a large value is comparable to that obtained for the single-crystalline CdSe

(36) Klebe, G.; Graser, F.; Hadicke, E.; Berndt, J. *Acta Crystallogr., Sect. B* **1989**, *45*, 69–77.
(37) Tojo, k.; Mizuguchi, J. *New Cryst. Struct.* **2002**, *217*, 517.
(38) Zuo, J. M.; Gao, M.; Tao, J.; lI, B. Q.; Twesten, R. D.; Petrov, I. *Microsc. Res. Technol.* **2004**, *64*, 347–355.
(39) Gao, M.; Zuo, J. M.; Twesten, R. D.; Petrov, I.; Nagahara, L. A.; Zhang, R. *App. Phys. Lett.* **2003**, *82*, 2703–2705.
(40) Cornil, J.; dos Santos, D. A.; Crispin, X.; Silbey, R.; Bredas, J. L. *J. Am. Chem. Soc.* **1998**, *120*, 1289–1299.

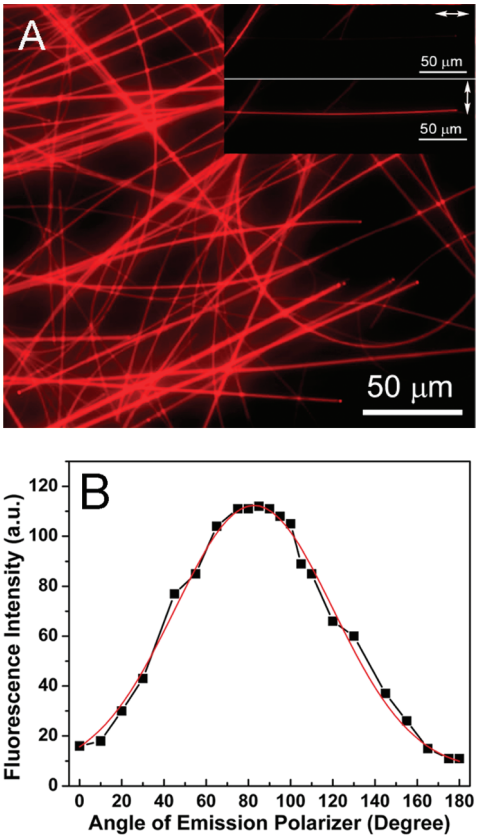

Figure 2. (A) Fluorescence microscopy image of nanobelts cast on glass slide. Inset: Polarized fluorescence images of a horizontally aligned nanobelt, where the arrows indicate the directions of the emission polarizer. (B) The fluorescence intensity as a function of the angle between the polarizer and the long axis of the nanobelt.

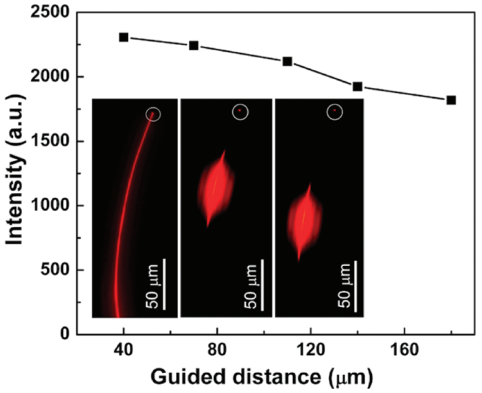

Figure 3. Intensity of the out-coupling light as a function of the guiding distance. Inset: (left) far-field fluorescence microscopy image of a single nanobelt, (middle and right) fluorescence images of the nanobelt obtained by excitation at different positions from the top end, where the waveguided emission spot was marked in the white circle. The light source is from a mercury lump, which was refined into a ~50 μm spot.

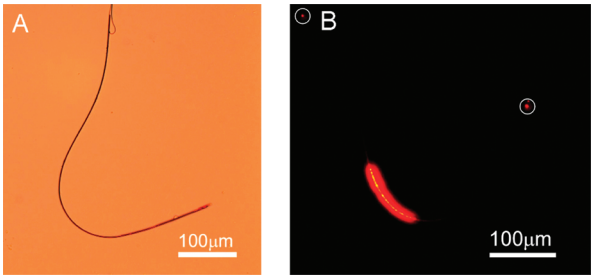

Figure 4. (A) Bright-field optical microscopy image of a bent nanobelt. (B) Fluorescence microscopy image of the bent nanobelt with excitation positioned at the curved part. The waveguided emission spot were marked in a white circle at the end of the nanobelt. The light source was from a mercury lump, which was refined into a ~50 μm spot.

nanorods, a highly fluorescent, linear polarized inorganic semiconductor.[41]

The 1D crystalline morphology of the nanobelts enables efficient waveguiding along the long axis of nanobelt, mainly because of the significant difference in refractive index between the nanostructures and its surroundings. As evidenced in Figure 3, the self-waveguided emission was imaged on a nanobelt with excitation spot (λ = 530−560 nm) positioned at different distances from the end of the nanobelt. No significant emission loss was observed within a long-range (> 100 μm) of light transportation. Such efficient waveguiding is likely due to the large Stokes shift of the fluorescence emission of the nanobelts (see Figure S6 in the Supporting Information), which in turn minimizes the light loss by self-absorption.[33] In contrast, significant overlap between the absorption and fluorescence band was often observed for many other organic, thus leading to dramatically decreased emission depending on the waveguiding distance.[8,9,34] One such example was found for the nanofibers fabricated from *para*-hexaphenyl molecules.[8,42] Although the single-crystalline phase was formed and strong emission polarization was also observed for the nanofibers, the intensity of the waveguided emission decreased exponentially with the waveguiding distance, mainly because of the self-absorption by the component molecules. The light scattering from bulk inhomogeneites and/or surface defects, which is usually dependent on the quality of the obtained materials, was another major cause for the waveguiding emission loss.[43] Pure crystalline structure is usually conducive for minimizing such scattering loss. To this end, molecular crystals are more favorable for employment as waveguides than the materials fabricated oligomers and conjugated polymers, which otherwise are difficult to grow into pure crystals mainly because of the complicated intermolecular interactions and polydispersity of the chains.

The efficient waveguiding of the nanobelts obtained in this study can even be observed with far-field excitation as shown in the large area imaging (Figure 2A), where bright spotty emission was clearly seen at the end of each of the nanobelts. The efficient waveguiding maintained even when the nanobelt was seriously bent (Figure 4), making it plausible to investigate the shape-dependent waveguiding of single nanobelt cavity in the similar manner as performed for the inorganic counterpart.[3] Such a bending-resistant waveguide may also find broad application in various optical or optoelectronic nanodevices where shape-flexible materials are needed.

(41) Hu, J.; Li, L.-S.; Yang, W.; Manna, L.; Wang, L.-W.; Alivisatos, A. P. *Science* **2001**, *292*, 2060–3.
(42) Balzer, F.; Bordo, V. G.; Simonsen, A. C.; Rubahn, H. G. *Phys. Rev. B* **2003**, *67*, 115408/1–115408/8.
(43) Di Benedetto, F.; Camposeo, A.; Pagliara, S.; Mele, E.; Persano, L.; Stabile, R.; Cingolani, R.; Pisignano, D. *Nat. Nanotechnol.* **2008**, *3*, 614–619.

The self-waveguiding observed is dependent on the cross-section size of the nanobelt. According to Balzer et al.'s model,[34,42] light propagation in 1D organic nanomaterials can be only in the transverse magnetic modes, and the number of light propagation mode, m, is restricted by[33]

$$m < \frac{2a}{\lambda} \cdot \frac{n_{\perp}}{n_{\parallel}} \sqrt{n_{\parallel}^{2} - n_{s}^{2}}$$

where α is the width of the nanobelt ($\alpha \approx 1000$ nm here), λ (630 nm) is the wavelength of the propagated light, $n_{\parallel}$ and $n_{\perp}$ are the refractive indices along and perpendicular to the nanobelt, respectively, and n_s (1.53)[33] is the refractive index of the glass substrate. Assuming $n_{\parallel}$ and $n_{\perp}$ are close to the value of 1.6 as obtained from a similar PTCDI molecule,[44] the number of the propagation mode can be calculated as $m < 1.5$, indicating only one allowable mode for the light propagation within the nanobelts reported here. This analysis suggests that nanobelts with smaller size will block the light propagation. Indeed, no waveguiding was observed for the nanobelts with size significantly smaller than ca. 400 nm. Moreover, nanobelts fabricated with tapered, sharp ends did not exhibit the outcoupling light at the end either (see Figure S8 in the Supporting Information).

(44) Gregg, B. A. *J. Phys. Chem.* **1996**, *100*, 852–859.

Conclusions

In conclusion, well-defined single-crystalline nanobelts with high fluorescence emission have been fabricated from a specifically modified PTCDI molecule, which affords flip-flap crystalline stacking. As demonstrated by the highly polarized and self-waveguided emission, these nanobelts will be of great interest for orientation-sensitive applications, such as polarized LEDs and nanolasers. Such practical applications will take additional advantages of the intrinsically high thermal and photostability of PTCDI materials.[6]

Acknowledgment. This work was supported by NSF (CAREER CHE 0641353, CBET 730667) and ACS-PRF (45732-G10). J.M.Z. was supported by U.S. Department of Energy (DOE) Grant DEFG02-01ER45923. Microscopy was carried out at the Center for Microanalysis of Materials at the Frederich Seitz Materials Research Laboratory, which is partially supported by DOE Grant DEFG02-91-er45439. Use of the Advanced Photon Source (APS) was supported by the DOE, Office of Science, Office of Basic Energy Sciences, under Contract DE-AC02-06CH11357. Technical onsite help with the APS facilities from Dr. Liang Guo is appreciated. L.Z. thanks the Utah Science Technology and Research initiative (USTAR) program for the support.

Supporting Information Available: Synthesis, nanobelt fabrication, SEM and TEM images, UV and fluorescence spectra, XRD data, and microscopy/spectroscopy characterization (PDF). This material is available free of charge via the Internet at http://pubs.acs.org.